# Geodynamic Generation of a Paleocene-Eocene Landscape Buried Beneath North Bressay, North Sea

Gaia Stucky de Quay[a], Gareth G. Roberts[b,*]

[a] *Department of Earth and Planetary Sciences, Harvard University, Cambridge, MA 02138, USA.*
[b] *Department of Earth Science and Engineering, Imperial College London, South Kensington Campus, SW7 2AZ, UK.*

**Abstract**

Histories of vertical lithospheric motions provide important clues about geodynamic processes. We present evidence of an ancient ($\sim 58 - 55$ Ma) landscape that likely uplifted and subsided rapidly during incipience of the Icelandic plume. Now buried beneath $\sim 0.4 - 0.8$ km of rock in the North Bressay region in the North Sea, this landscape is located within a sedimentary basin on the margin of the North Atlantic Ocean. We use high-resolution 3D seismic reflection data to map this ancient surface. Correlation of stratigraphy with a survey in the Bressay region constrains age and depositional environment. The landscape contains excellent evidence of meandering fluvial channels, some of which record avulsions, and terminate against a coastline to the east where deltaic landforms are identified. The landscape was depth-converted and decompacted to generate a digital elevation model from which river profiles were extracted. Their geometries indicate that the landscape was generated by three phases of uplift. This history of uplift and subsidence is analogous to similar-aged landscapes in the Judd area $\sim 400$ km to the west and Bressay $\sim 30$ km to the south, and appears to be another manifestation of lithospheric motions generated by the passage of warm thermal anomalies away from the Icelandic plume.

*Keywords:* Buried landscape, Icelandic plume, Paleogene, North Atlantic,

*Corresponding author
*Email address:* gareth.roberts@imperial.ac.uk (Gareth G. Roberts)

Mantle convection, Fluvial erosion

## 1. Introduction

Histories of vertical lithospheric motions are important constraints for identifying processes responsible for driving Earth's surface evolution over geological timescales (e.g., shortening, extension, mantle convection). Presently, the North Atlantic Ocean hosts a region of mantle convective upwelling centered on Iceland, resulting in 1–2 km of dynamic support and elevated continental margins at its fringes (e.g. White & McKenzie, 1989; Rickers et al., 2013; Hoggard et al., 2016). The composition and age of basaltic magmatism, V-shaped ridges south of Iceland, topographic, stratigraphic, tomographic and thermochronologic observations have provided insights into the plume's evolution since its formation $> 60$ Ma (e.g. Lawver & Müller, 1994; Saunders et al., 1997; Japsen & Chalmers, 2000; Jones et al., 2002; Mudge & Jones, 2004; Storey et al., 2007; Shaw Champion et al., 2008; Parnell-Turner et al., 2014; Schoonman et al., 2017; Hardman et al., 2018). Nonetheless, we have a limited understanding of its planform through time or the influence of temporal fluctuations. One way to probe the evolution of the Icelandic plume at greater spatial and temporal resolutions is through the identification and study of buried terrestrial landscapes that were once uplifted by thermal anomalies sourced from the ancient plume (e.g. Underhill, 2001; Shaw Champion et al., 2008; Hartley et al., 2011; Stucky de Quay et al., 2017; Conway-Jones & White, 2022).

The Faeroe-Shetland, Moray Firth, and North Sea basins display stratigraphic records containing coarse Paleocene-Eocene terrestrial sandstones sandwiched between marine mudstones. Such observations indicate that these regions experienced short-lived ($< 3$ Ma) histories of marine-terrestrial-marine conditions close to the Paleocene-Eocene boundary (e.g. Mudge & Bujak, 2001; Underhill, 2001; Mudge & Jones, 2004; Mackay et al., 2005; Shaw Champion et al., 2008; Hardman et al., 2018; Jolley et al., 2021; Conway-Jones & White, 2022). There is ongoing debate about the contributions of plate tectonic pro-

cesses (e.g. shortening and extension) and sub-plate support in generating vertical motions in these areas (see e.g. Jolley et al., 2021). However, the amplitudes of uplift (up to $\sim$ 1 km), combined with its rapidity and, importantly, subsequent subsidence, indicates that these vertical motions cannot be attributed to glacio-eustasy, magmatic underplating, nor crustal tectonics (e.g., shortening, extension). Instead, they have been attributed to the passage of thermal, buoyant, anomalies in a low viscosity channel beneath the lithosphere away from the centre of the Icelandic plume (e.g., Shaw Champion et al., 2008; Rudge et al., 2008).

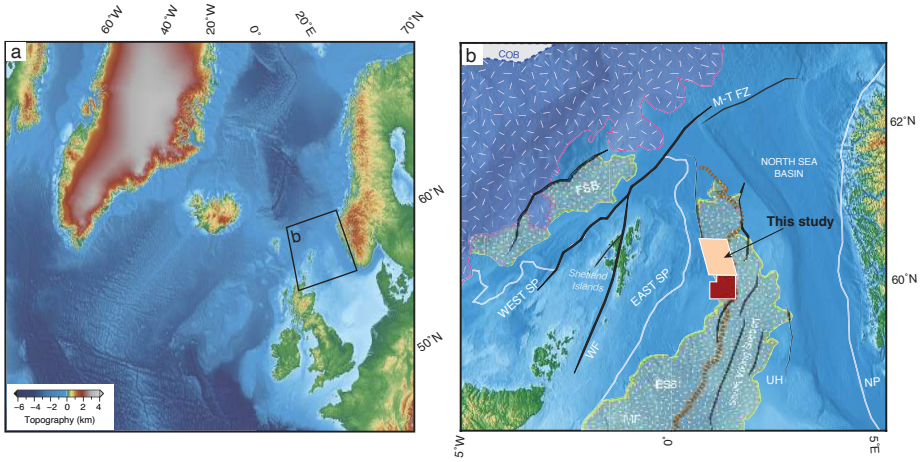


Figure 1: **North Bressay study site**. (a) Location of North Bressay relative to present-day geography of the North Atlantic Ocean. (b) North Bressay and its surroundings between Scotland and Norway. Red/orange polygons = Bressay/North Bressay 3D seismic datasets. Pink edged polygon = Paleocene lavas; yellow stippled areas = slope and basin sands; orange dashed line = eastern limit of the Dornoch delta; black lines = faults; COB = continent-ocean boundary; FSB = Faeroe-Shetland Basin; SP = Shetland Platform; M-T FZ = Møre-Trøndelag Fault Zone; ESB = East Shetland Basin; WF = Walls Fault; UH = Utsira High; NP = Norwegian Platform (Mudge, 2015).

In the Judd region, located in the Faroe-Shetland basin, an erosional unconformity has been mapped at the base of the coarse sandstone Flett Formation (Smallwood & Gill, 2002; Shaw Champion et al., 2008). Depth conversion and

decompaction of infilling stratigraphy and recorded lignite suggests that the unconformity was created by erosion of a terrestrial landscape with at least 900 m of relief (Shaw Champion et al., 2008; Hartley et al., 2011). Dinoflagellate and pollen chronostratigraphy indicate that this landscape formed by $\sim 55$ Ma. Jolley et al. (2021) suggest that the unconformity might be a composite of two erosional surfaces that formed as a result of two phases of uplift between $\sim 58 - 56$ Ma. Longitudinal profiles extracted from this surface have almost 1 km of relief and contain three large ($> 100$ m of relief) knickzones (Hartley et al., 2011). Two younger and two older ($\sim 61.5 - 52.5$ Ma) landscapes that each grew and were buried in a few million years have been mapped in the Judd area (Conway-Jones & White, 2022). The history of vertical motions inferred from these observations and from similar aged stratigraphy in surrounding regions has been interpreted as a record of thermal perturbations of the Icelandic plume (see e.g. Conway-Jones & White, 2022, their Section 2.5, for a recent summary).

To the east, in the Bressay region of the North Sea, a similar aged ($\sim 58-55$ Ma) terrestrial landscape, now buried by $\sim 1.5$ km of rock, has been identified in well and seismic data (Figure 1; Underhill, 2001). The Bressay region is located on the East Shetland Platform of the northern North Sea. Buried extensional faults and backstripped well data indicate that the East Shetland platform was stretched by a factor $\beta = 1.3 \pm 0.04$ from the Late Jurassic for $\sim 60$ Ma (White, 1990; Underhill, 2001). It currently sits on the eastern fringe of the Icelandic plume (Rickers et al., 2013; Hoggard et al., 2016). Cuttings from wells that intersect the $\sim 58-55$ Ma landscape contain angiosperm (flowering plant) debris, which, combined with mapped dendritic drainage patterns and coarse clastic material, indicate that it formed subaerially (Stucky de Quay et al., 2017). Similar to the Judd area, longitudinal river profiles extracted from this landscape contain three broad knickzones, which do not correlate with substrate, and instead indicate a staged uplift history. Dinoflagellate cysts in the marine stratigraphy below and above the landscape indicate that it formed in

less than 3 Ma and was rapidly drowned, again similar to the Judd area. These buried landscapes, scattered across fringes the North Atlantic Ocean, thus provide an opportunity better constrain Icelandic plume activity by providing multiple points of reference in space and time.

This study describes a hitherto unmapped Early Paleogene eroded surface $\sim 30$ km north of the Bressay buried landscape (herein termed the North Bressay region; see Figure 1). Similar to other sedimentary basins on the fringes of the North Atlantic Ocean, it contains stratigraphic evidence of rapid uplift, landscape evolution and subsidence during incipience of the Icelandic plume (e.g. Underhill, 2001; Shaw Champion et al., 2008; Rudge et al., 2008; Hartley et al., 2011; Stucky de Quay et al., 2017; Jolley et al., 2021). In the following sections we first describe seismic data and examine stratigraphic, tectonic and geomorphic observations from the North Bressay area. We then extract, depth-convert, and decompact a prominent erosional surface, which we tentatively assign an age based on correlation with stratigraphy in the Bressay area to the south. Drainage networks are extracted from this landscape and longitudinal river profiles are inverted for a history of uplift. Finally, we discuss implications of the calculated uplift histories for evolution of the region during the initial stages of the Icelandic plume.

## 2. Seismic data and stratigraphic correlation

A high-resolution, three-dimensional seismic survey (MC3D-ESP2015M) located directly north of the Bressay region was made available for the study by PGS (Petroleum Geo-Services) and Equinor. Dendritic and meandering drainage, unconformities and shallower (younger) polygonal faulting in North Bressay stratigraphy are clearly visible in slices through seismic variance (trace-to-trace variability; Figure 2a-b). The meandering drainage networks at a depth of $\sim 600$ ms (two-way time) coincide with the strongest reflector visible in the seismic

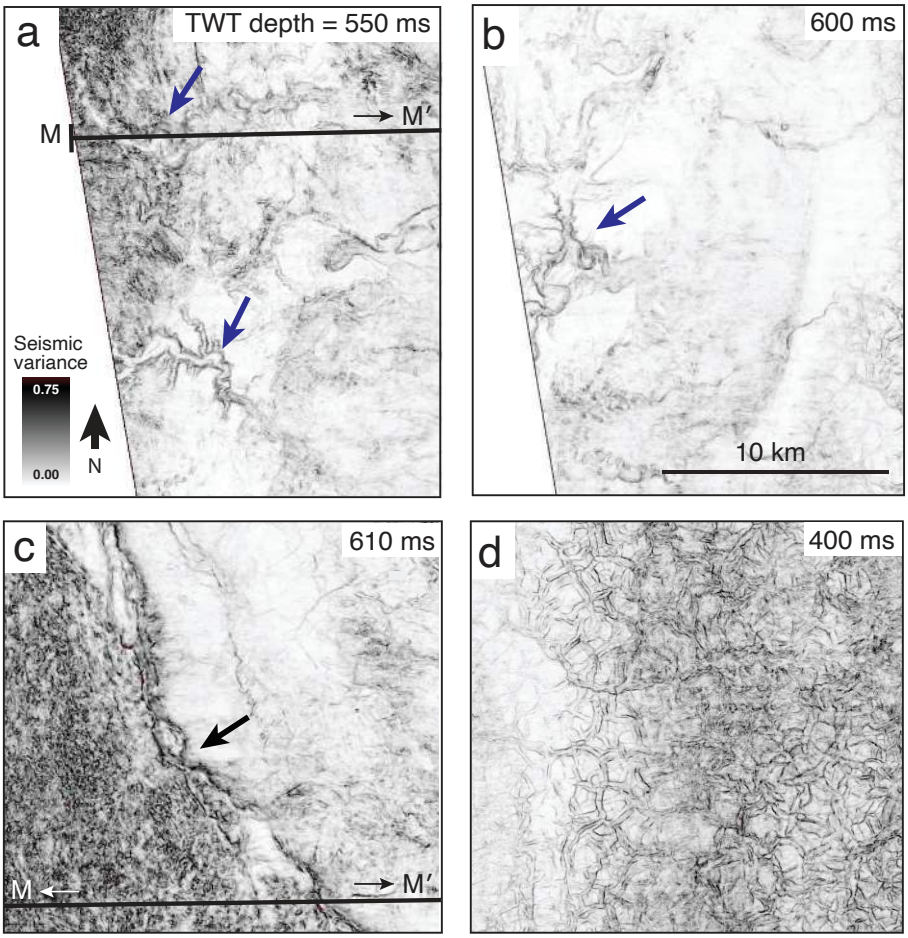


Figure 2: **North Bressay geomorphology and structural features visible in seismic variance depth slices.** (a-b) Blue arrows = meandering channels. (c) Black arrow = large unconformity. (d) Pervasive polygonal faulting. TWT depth = Depth of slice through seismic variance cube at two-way time indicated in milliseconds. M—M′ = location of cross-section shown in Figure 3.

cross-section shown in Figure 3a, where evidence for valley incision can also be observed (see red arrows in Figure 3b).

In order to characterize the stratigraphy, well logs within the MC3D-ESP2015M seismic survey were also made available. However, their location to the east of a large unconformity (Figure 2c, 3) mean that direct stratigraphic correlation between the wells and the eroded surface to the west is challenging. Fortunately, this survey abuts the northern edge of the PGS BBK survey, which was used to map a $\sim 58 - 55$ Ma buried landscape in the Bressay region (Stucky de Quay et al., 2017). This previous study incorporated seven wells that intersect the eroded landscape and stratigraphy located towards the south. The well reports contained geophysical data (e.g., checkshots, gamma-ray logs) and biostratigraphic observations that were used to depth-convert seismic data, calibrate compaction parameters and quantify the age of stratigraphy and its uncertainties. The reader is referred to Stucky de Quay et al. (2017, and references therein) for detailed lithological and biostratigraphic descriptions and detailed age constraints. Similarities in acoustic impedance contrasts (e.g. seismic facies) between the MC3D-ESP2015M and BBK surveys give a basis for interpreting the stratigraphy in western North Bressay and for depth-converting and decompacting its stratigraphy using similar techniques.

Correlation of seismic stratigraphy indicates that the prominent incised layer at $\sim$ 600 ms in North Bressay is of Lower Cretaceous age (Cromer-Knoll-Shetland Group; Figure 3). Overlying deposits are likely to be the Paleocene-Eocene aged Moray and Montrose Groups (cf. Bressay and Judd chronostratigraphy in Stucky de Quay et al., 2017, their Figure 2). Well logs in the Bressay area suggest the incised Cretaceous layer is composed of limestones and is overlain by interbedded sand and shales containing coarse, pebbly, sandstone (see Stucky de Quay et al., 2017, their Figure 4). Acoustic impedance contrasts within the Montrose and Moray Groups are suggestive of interbedded sands, shales and conglomerates (Figure 3). Above the Montrose and Moray Group,

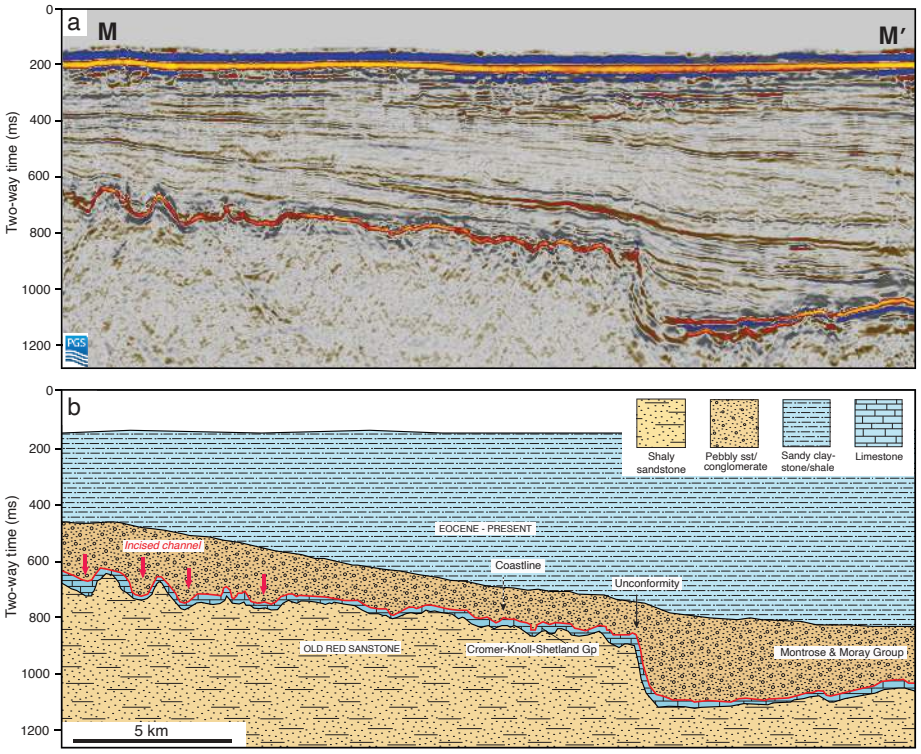


Figure 3: **Interpreted seismic stratigraphic section of the North Bressay region.** (a) Example of a vertical seismic slice through 3D seismic volume along M—M′ trace (see Figure 5) and (b) interpreted stratigraphy. Data courtesy of PGS (survey MC3D-ESP2015M).

a succession of undifferentiated marine mudstones is mapped up to the seabed (Figure 3b). Below Cretaceous stratigraphy in the Bressay area, the logs report sandstones, which are most likely of the Old Red Sandstone (Devonian) Group. Figure 4 shows a tentative interpretation of Paleocene-Eocene chronostratigraphy for North Bressay compared to the Bressay and Judd regions (after Shaw Champion et al., 2008; Stucky de Quay et al., 2017; Jolley et al., 2021). The fidelity of interpreted North Bressay stratigraphy could obviously be assessed and improved if data from wells penetrating the erosional surface become available.

## 3. Buried North Bressay Landscape

### *3.1. Seismic mapping*

The strong reflector at $\sim$ 600 ms in Figure 3a was mapped in two dimensions with a horizontal resolution of $\sim$ 10 m. Results using auto-tracking and manual mapping of in-lines and cross-lines yield similar results due to the continuity of the mapped surface. The resulting mapped surface in two-way time is shown in Figure 5. It contains a dendritic drainage system in the northwest comprising multiple tributaries. Unlike Bressay, these channels show evidence of $<$ O(1 km) meandering. Overlapping and interconnected meanders record channel avulsion events (e.g., southernmost channel in Figure 5). The channels drain from higher elevations ($\sim$ 600 ms below sea level; $\sim$ 400 ms below seabed) toward the east ($>$ 800 ms below sea level). Incised valleys appear to stop along a palaeo-coastline, and localised deposits at the mouths of channels are most likely deltaic in origin (blue arrow in Figure 5). These geomorphologic features, combined with stratigraphic evidence for coarse fluvial sediments in overlying sediments, are suggestive of formation in a subaerial environment akin to the erosional landscape mapped at a similar stratigraphic level in the Bressay region. Preservation of meandering channels, interfluves, deltaic deposits and overlying sedimentary deposits suggests rapid burial and modest erosion during marine

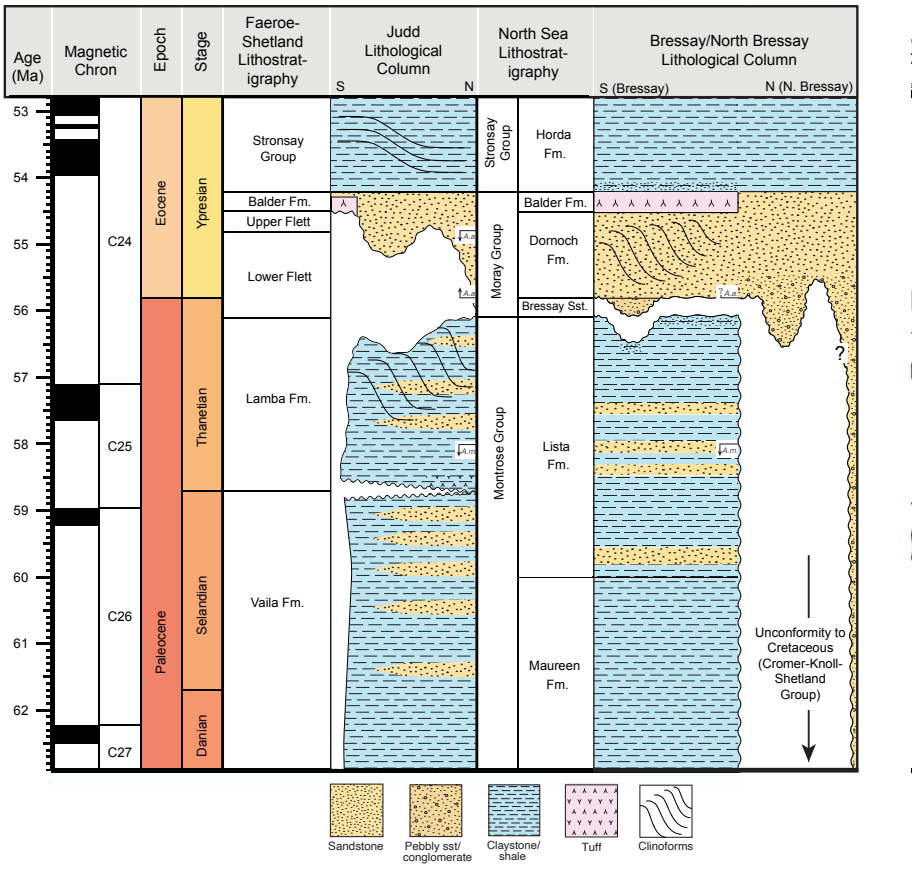


Figure 4: **Paleocene-Eocene chronostratigraphy of North Bressay, Bressay and Judd regions.** Judd stratigraphy after Shaw Champion et al. (2008), see also Jolley et al. (2021). Bressay stratigraphy after Stucky de Quay et al. (2017). Chronostratigraphy for North Bressay region (this study) is based on correlating seismic facies with the Bressay region to the south. Ages for dinocysts Apectodinium augustum (A.a) and Alisocysta margarita (A.m) are from Luterbacher et al. (2004).

transgression. We note that quasi-linear depressions are observed between the mapped coastline and unconformity (Figure 5: dashed and solid lines). They do not obviously link with the meandering channels mapped upstream. We note that they sit between depositional highs, which we interpret as deltaic deposits. We are therefore cautious about interpreting them as downstream fluvial reaches and instead tentatively suggest that they might be marine channels.

### *3.2. North Bressay vs. Bressay buried landscapes*

The Bressay and North Bressay drainage systems are located $\sim$ 30 km apart. They share commonalities in their morphology including incised valleys sloping eastward toward paleo-coastlines, and appear to contain similar stratigraphy, including coarse, pebbly, channel infill. Stratigraphic correlations indicate that they are of a similar, late Paleocene to early Eocene, age (Figure 4). The North Bressay landscape has a larger extent, greater resolution and more clearly defined valleys than the Bressay landscape. It contains a greater number of individual basins, channels, and tributaries as well as evidence of coeval deposits at the valley mouths. Due to its biostratigraphic records and abundance of available intersecting cores, data from the the Bressay area were used to depth-convert, decompact, and constrain the evolution of the North Bressay landscape in the following section (Stucky de Quay et al., 2017).

Notwithstanding these similarities, we note that are there subtle but important differences between the two landscapes and data sets. First, the Bressay landscape sits below prominent gas columns that partially obscure deeper stratigraphy—they are far less prominent/absent atop the North Bressay landscape. Secondly, the MC3D-ESP2015M survey does not extend far enough to the west for river heads to be mapped. Despite these challenges, the proximity of the nearby Bressay region provides an opportunity to constrain the relief of the North Bressay landscape as it formed and a tentative assessment of its uplift and erosional history.

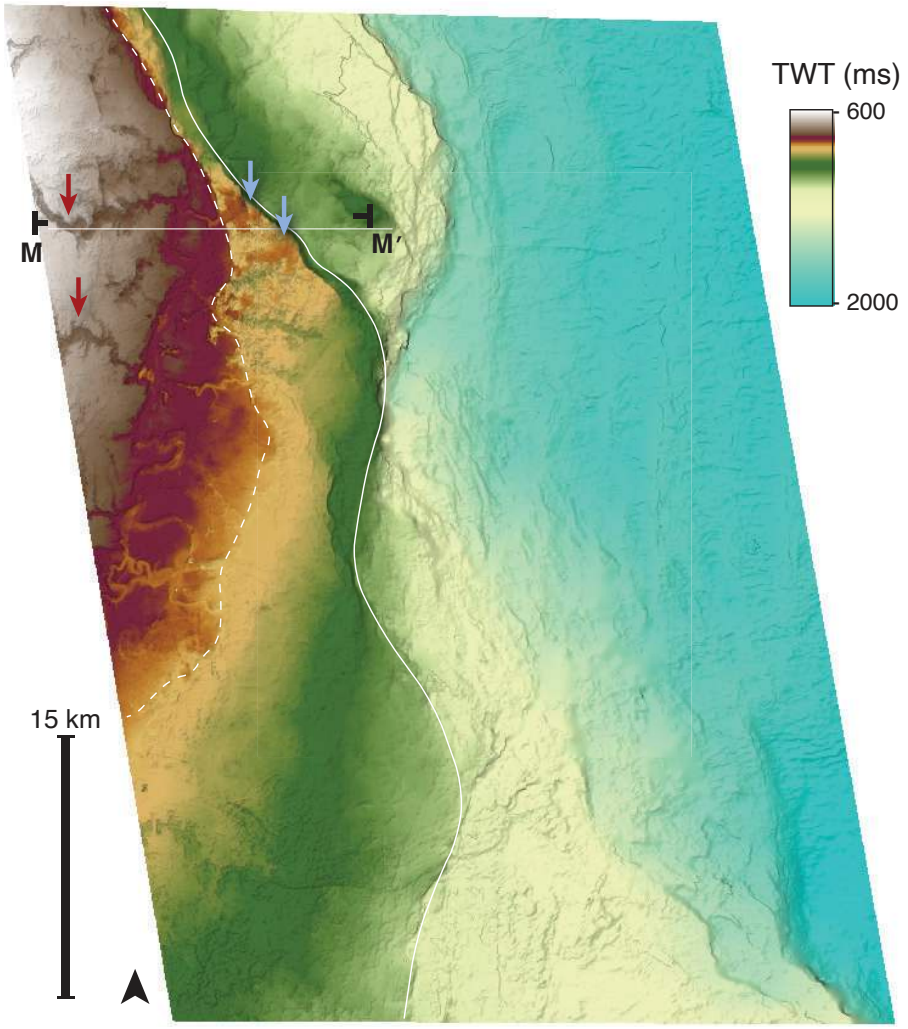


Figure 5: **North Bressay channelised surface.** This ∼ 58 Ma surface was mapped at a horizontal resolution of ∼ 10 m using in-lines and cross-lines from the MC3D-ESP2015M seismic survey. It corresponds to the bright reflector visible in the seismic cross-section shown in Figure 3a, atop which evidence for valley incision is observed. Red arrow = incised channels. White dotted line = palaeo-coastline. Light blue arrow = depositional features. Solid white line = unconformity. M—M′ = location of cross-section shown in Figure 3.

*3.3. Depth conversion and decompaction*

Five wells in the Bressay area had check-shot data available, which range from zero to $\sim$ 1200 ms ($\sim$ 1400 m) below the seabed. These data were used to constrain the following optimal relationship between two-way time ($t$, milliseconds) and depth ($z$, meters),

$$z = 0.0164t^2 + 0.8719t. \tag{1}$$

Equation 1 fits the available check-shot data with an $r^2 = 0.99$ (see Stucky de Quay et al., 2017, their Figure 9a). One standard deviation was used to assess uncertainties in calculated depths.

The depth-converted landscape was corrected for post-depositional compaction using a simple, widely-used, parameterisation of porosity ($\phi$),

$$\phi(z) = \phi_\circ \exp\left(-z/\lambda\right), \tag{2}$$

where $\phi_\circ$ is initial porosity (e.g. at the seabed), $\lambda$ is compaction wavelength and $z$ is depth. Values of compaction parameters ($\phi_\circ$, $\lambda$) were estimated by fitting check-shot data using an empirical relationship that includes depth, velocity and compaction parameters, which yielded optimal (best-fitting) parameters of $\phi_\circ = 0.77$ and $\lambda = 2.4$ km (Wyllie et al., 1956; Sclater & Christie, 1980; Christensen, 1982; Czarnota et al., 2013). Note that, although a global minima is identified, $\phi_\circ$ and $\lambda$ trade-off, which impacts assessment of uncertainties in compaction parameters (see Stucky de Quay et al., 2017, their Figure 9b-c). Decompaction was performed assuming that the solid grain fraction is conserved, i.e. $\int 1 - \phi(z)\mathrm{d}z$ is the same between compacted and decompacted columns. Depositional thickness, $z_3$, is given by solving the integrals to yield,

$$z_3 = z_2 - z_1 - \phi_\circ\lambda\left[\exp(-z_1/\lambda) - \exp(-z_2/\lambda) + \exp(-z_3/\lambda) - 1\right], \tag{3}$$

where $z_2 - z_1$ is the compacted thickness of the layer and $z_3$ is its depositional thickness. Note that $z_3$ appears on both sides of the equation, which was solved by Newton-Raphson iteration, we set $z_3 = z_2 - z_1$ in the first iteration, values of $z_3$ tend to converge to 3 d.p. by 3–5 iterations (see e.g. Stucky de Quay et al., 2017, for details). The depth-converted and decompacted eroded surface is shown in Figure 6a. Uncertainties in relief ($\sim \pm 20$ m) vary as a function of the velocity model and compaction parameterisation. The total relief of the landscape is $\sim 500$ m, and contains evidence of rivers draining east towards a palaeo-coastline.

### *3.4. Drainage patterns*

In order to recreate the landscape's hydrology at the time of subaerial exposure, Esri flow routing algorithms were used to extract drainage networks from the mapped landscape (Figure 6a). First, flow directions were calculated using the steepest descent from each cell in the digital elevation model of the landscape (Tarboton, 1997). Subsequently, flow accumulation to each cell was measured and flow lengths were calculated. Drainage networks were extracted from the six main basins and a subset of 107 longitudinal river profiles (elevation as a function of distance) were generated (Figure 6b–g). The extracted drainage patterns highlight the presence of eastward flowing, dendritic and meandering networks atop the eroded landscape. The mapped rivers are up to $\sim 13$ km long and have a maximum relief of $\sim 380$ m. Stucky de Quay et al. (2017) showed that uncertainties in the velocity model and compaction parameters stretched or compressed calculated river profiles (vertically) by $\pm 25$ m and that the location and relief of knickzones are largely unaffected by these uncertainties. We therefore extract longitudinal river profiles from the digital elevation model produced using the optimal velocity model and compaction parameters.

The river profiles shown in Figure 6b–g are all broadly convex-upward and most contain large knickzones with relief up to O(100 m). The geometries of

these profiles indicate that the landscape was eroding in response to changes in its history of uplift before it was rapidly drowned and buried by sediment (see e.g. Rosenbloom & Anderson, 1994; Howard et al., 1994; Whipple & Tucker, 1999; Pritchard et al., 2009). The mapped surface is essentially a snap-shot of a short-lived (< few Ma) evolving landscape. In the following section we invert the four longest complete longitudinal river profiles for a history of uplift of the North Bressay landscape.

## 4. Uplift histories from inverse modelling

Pritchard et al. (2009) and Roberts & White (2010) showed that longitudinal river profiles could be successfully inverted for a history of uplift rate. Following Stucky de Quay et al. (2017), we use a simplified version of the stream power model to invert rivers draining the North Bressay landscape for uplift rate, $U$, as a function of time, $t$,

$$\frac{\partial z}{\partial t} = U(t) - vA(x)^m \frac{\partial z}{\partial x}, \tag{4}$$

where erosion rate, $\partial z/\partial t$, is parameterised using the advective term on the right-hand side of Equation 4. This term controls the velocity of kinematic erosional waves as they propagate upstream (e.g., Rosenbloom & Anderson, 1994; Whipple & Tucker, 1999). In this parameterisation, erosional velocities, and ultimately the duration of landscape response to uplift, depend on upstream drainage area, $A$, which is measured from the extracted landscape, and the values of the erosional parameters, $v$ and $m$. $z$ is elevation and $x$ is distance along the river.

The lack of direct biostratigrapic control means that the age of the channelized North Bressay surface cannot be constrained with the precision of the Bressay and Judd areas. However, the overlying sedimentary rock appears to be

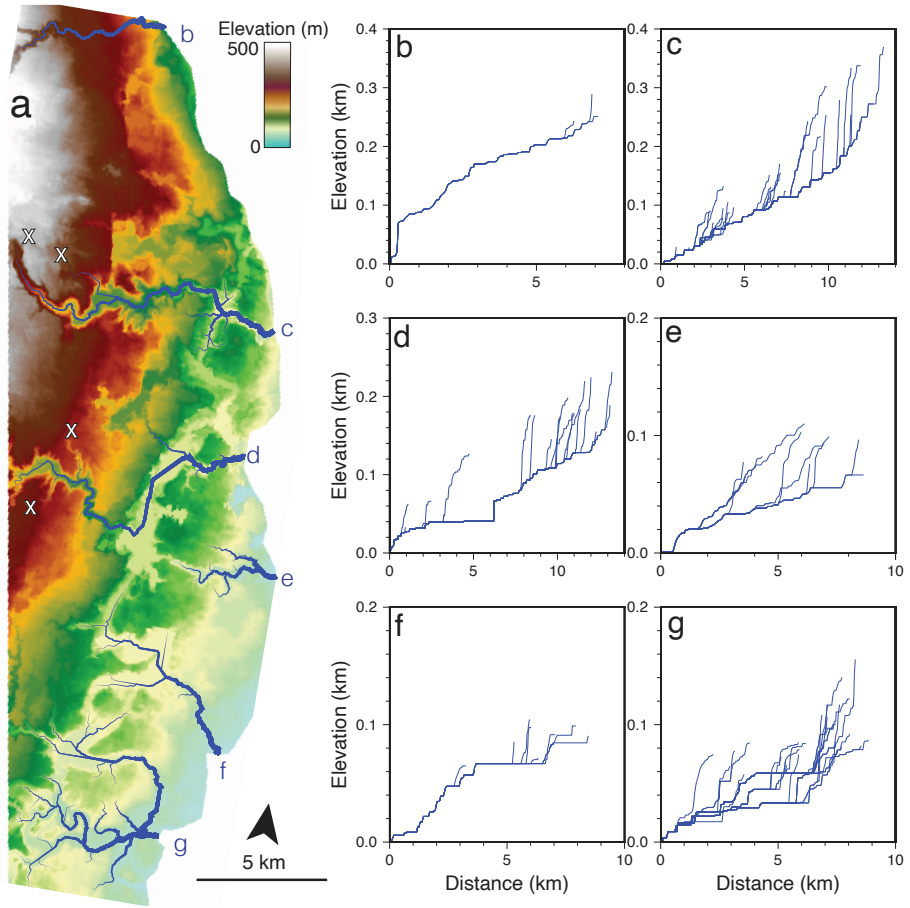


Figure 6: **Reconstructed North Bressay erosional surface, drainage networks, and longitudinal profiles.** (a) Depth-converted and decompacted North Bressay landscape. Blue lines = drainage extracted from six main basins (annotated: b-g). X labels indicate rivers inverted for histories of uplift (Figure 7). (b-g) Longitudinal profiles of rivers (N = 107) in North Bressay grouped by basins annotated in (a).

of a similar age to sediments that infilled the Bressay landscape (Late Paleocene-Early Eocene). Since there are no other heavily channelized surfaces in either region, and considering their proximity (∼30 km), presence of infilling coarse sandstones and comparable palaeo-coastlines, we consider it likely that they they formed in a similar way (subaerially) around the same time. The biostratigraphic records discussed previously indicate that the duration of exposure is $< 3$ Ma. Joint inverse modelling of the Bressay drainage inventory indicates that the best-fitting value of erosional parameter $m = 0.5$. Calibrated values of $v$ in the Judd and Bressay regions are 4.75±0.1 $\mathrm{Ma}^{-1}$ and 1.6±0.1 $\mathrm{Ma}^{-1}$, respectively (Hartley et al., 2011; Stucky de Quay et al., 2017). We invert North Bressay river profiles for histories of uplift using this range of erosional parameter values.

The inverse problem is solved by seeking the minimum value of the objective function, $H$, which incorporates data (root mean squared, rms) misfit, model roughness, and a positivity penalty function, $P$,

$$H = \left[ \frac{1}{N} \sum_{i=1}^{N} \left( \frac{z_i^o - z_i^c}{\sigma_i} \right)^2 \right]^{1/2} + \frac{W_1}{M-1} \sum_{k=2}^{M} U' + \frac{W_2}{M} \sum_{k=2}^{M} U'' + \frac{W_3}{M} \sum_{k=1}^{M} P, \quad (5)$$

where $N$ is the total number of measurements of elevation and distance in the drainage inventory. Data variance $\sigma_i$ is set to 20 m, which is a conservative estimate of the vertical resolution of the seismic data. In practice the model seeks the smoothest uplift rate history that yields the lowest residual misfit between observed and theoretical river profiles (Parker, 1994; Roberts & White, 2010). $U'$ and $U''$ are the first and second derivatives of calculated uplift, which is parameterised by selecting $M$ discrete values (see Roberts & White, 2010). Consistent with Stucky de Quay et al. (2017), we set smoothing parameters, $W_n = 0.1$. The positivity penalty function $P = \cosh(U) - 1$ if $U < 0$, $P = 0$ if $U \geq 0$. The model uses Powell's algorithm, a conjugate gradient method, to invert for uplift rate histories, which yields stable solutions (Roberts & White, 2010; Hartley et al., 2011; Stucky de Quay et al., 2017). In the starting model

$z(x) = 0$ and $U(t) = 0$. Two rivers from the two largest basins were jointly inverted for their uplift rate histories (Figure 6a).

Residual misfit between observed (black curves) and best-fitting theoretical (red curves) river profiles is low (rms $\sim 1$; Figure 7a, c). Changing the value of erosional parameter $v$ scales the timing of calculated uplift. As expected, the relatively low value of $v = 1.6$ Ma$^{-1}$ (calibrated in the Bressay region) results in a calculated uplift history that is $\sim 3$ times longer-lived than when the faster velocity, based on calibration from the Judd area: $v = 4.75$ Ma$^{-1}$, is used (cf. black & grey curves in Figure 7b, d). Given the proximity of the study area to Bressay, we favour the slower advective velocity $v$, which we note yields broadly similar uplift histories to those calculated using rivers in the Bressay area (cf. Stucky de Quay et al., 2017, their Figure 12b). However, we acknowledge that both parameterisations yield uplift histories $< 3$ Ma in duration and that no direct biostratigraphic control means that evidence to discriminate between the two uplift histories is lacking.

## 5. Discussion

Seismic reflection data in the North Bressay region of the North Sea contain evidence of an ancient fluvial landscape now buried beneath $\sim 0.4 - 0.8$ km of marine deposits. The quality of the survey permits extraction of a high-resolution, O(10 m), digital elevation model of the landscape. Correlation of stratigraphy observed within this survey and an adjacent survey in the Bressay region indicate that the landscape formed close to the Paleocene-Eocene boundary ($\sim 55$ Ma) within a few million years ($< 3$ Ma). Mapped meandering rivers show evidence of avulsion in the southern sector of the survey. The rivers appear to terminate in the east against what we have mapped as an undulating coastline. At least two deltaic landforms abut the mouths of rivers mapped in the northern section of the survey. The fluvial landscape extended beyond the

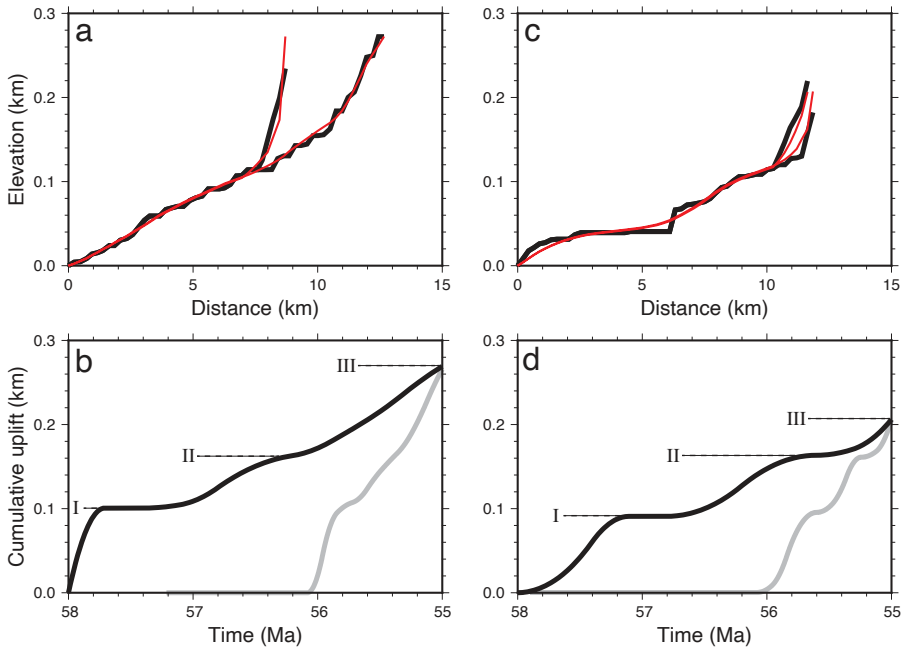


Figure 7: **Uplift histories from inverse modelling of river profiles.** Joint inversion of rivers from the two largest basins in North Bressay for uplift rate as a function of time. (a) Two largest rivers in basin c (see Figure 6). Black = observed river profiles. Red = best-fitting theoretical profiles. (b) Cumulative uplift histories that produced theoretical profiles shown in panel (a). Black and grey curves = uplift histories generated when erosional parameter $v$ = 1.6±0.1 $Ma^{-1}$ and 4.75±0.1 $Ma^{-1}$, respectively. Uplift events are labeled I, II, III. (c-d) Longitudinal profiles and calculated cumulative uplift for two longest rivers in basin d (Figure 6).

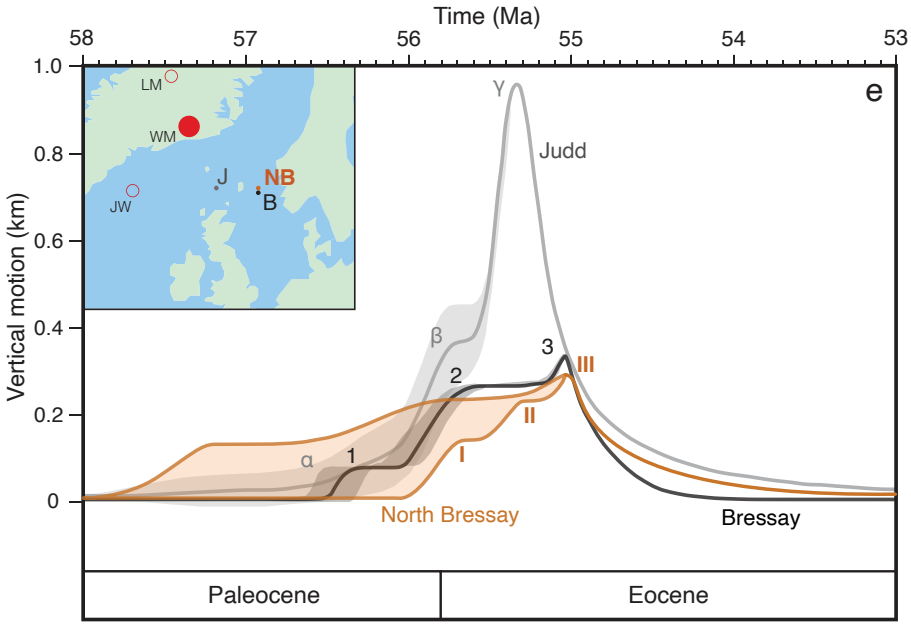


Figure 8: **Uplift histories of North Atlantic Paleocene-Eocene landscapes**. Shaded bands = uncertainty from erosional parameter values. I, II, II = North Bressay uplift events (this study); 1, 2, 3 = Bressay uplift events (Stucky de Quay et al., 2017); $\alpha$, $\beta$, $\gamma$ = Judd uplift events (Hartley et al., 2011). Inset depicts Paleocene-Eocene paleogeography showing location and approximate extent of the uplifted regions discussed here: orange/black/gray circles = North Bressay (NB), Bressay (B), and Judd landscapes (J); large red circle labelled WM = Icelandic plume center from White & McKenzie (1989); LM/JW = plume centers from Lawver & Müller (1994)/Jones & White (2003).

western limit of the survey (see Figure 5).

Inverse modeling of the two largest river systems extracted from the landscape indicates that fluvial geometries are best explained by uplift occurring in three distinct stages (I, II, and III); this is strikingly analogous to uplift histories calculated by inverting river profiles from similar aged (now buried) landscapes $\sim 30$ km to the south (Bressay) and $\sim 400$ km to the west (Judd; Figure 8). Rapid uplift and subsidence of these landscapes indicates that neither glacio-eustasy, which is too small amplitude, underplating, which generates uplift but no/very little subsidence, nor crustal tectonics (e.g., shortening followed by extension), played a governing role in generating the landscape. Instead simple isostatic calculations indicate that these landscapes could have been generated by the passage of a warm thermal anomaly ($\sim 130 - 50$°C excess temperature) away from the Icelandic plume in a low viscosity channel beneath the plate (Rudge et al., 2008).

The proximity of North Bressay to Bressay, and their stratigraphic similarities, indicate that uplift may also have been generated by the passage of a warm thermal anomaly beneath the plate in $\sim 1-3$ million years. If we assume isostasy prevails and that compressibility is negligible, the average excess temperature in a low viscosity channel, $\overline{T}$, required to generate the observed uplift, $u$ is given by

$$\overline{T} = \frac{u}{h}\left[\frac{1}{\alpha} - T_{\circ}\right], \tag{6}$$

where $h$ is the thickness of the anomalously warm layer, $T_{\circ}$ is background temperature, and $\alpha = 3.28 \times 10^{-5}$ K$^{-1}$ is thermal expansivity. If the background temperature of the plume head is 1400°C and the thickness of the hot layer is 200 km, an excess temperature of 44°C is required to generate the $\sim 300$ m of uplift predicted by inverting river profiles. Note that this calculation is insensitive to assumed background temperature. The calculated excess temperature is within the range of values estimated for similar ($\sim 61.5 - 52.5$ Ma), now buried,

landscapes in the Judd area (16–120°C; Conway-Jones & White, 2022).

We tentatively suggest that the buried landscape mapped in this study is another record of rapid transient vertical motions generated by mantle convection (Figure 9). Mapping of ancient buried landscapes is a rich source of geomorphological information including constraints on erosion rates and planform responses to rapid uplift and subsidence. The discovery and analysis of spatially distributed buried landscapes through seismic mapping holds great potential for providing quantitative constraints on the timing and extent of the Icelandic plume through time.

## 6. Conclusions

In this study we present a newly identified and previously unmapped ancient buried landscape located in the North Bressay region of the northern North Sea. The landscape was identified by mapping seismic reflectors on a three dimensional survey provided by PGS and Equinor. It contains excellent evidence of well-preserved, incised meandering channels, avulsion, and a palaeo-coastline with deposition of sediments in deltas. Correlation of stratigraphy in the region with an existing survey to the south indicates that the eroded surface was terrestrial and formed in a few million years between $\sim 58 - 55$ Ma. Longitudinal river profiles extracted from the depth-converted and decompacted landscape contain convex-upward reaches, which indicate that the landscape was youthful when it was subsequently buried by marine sediment during subsidence. Inverse modeling of the longitudinal profiles indicates that uplift of the landscape occurred in three stages, similar to uplift histories calculated for similar aged landscapes in the Judd area $\sim 400$ km to the west and Bressay $\sim 30$ km south. The uplift and subsidence history of the North Bressay landscape is consistent with the notion that excess thermal anomalies travelling beneath the plate away from the Icelandic plume generated rapid Paleocene-Eocene lithospheric uplift

and subsidence.

**Acknowledgements and Data Availability**

G. Stucky de Quay was supported by the National Environmental Research Council (NERC) Grantham Institute SSCP DTP (grant number NE/L002515/1). Seismic and well data were made available by PGS (survey MC3D-ESP2015M) and Equinor, we thank them for their help. Requests for access to seismic data should be made to PGS (Petroleum Geo-Services). Data, input files and source code for the inverse models are available from the authors. We thank R. Bell, C. Jackson, G. Hampson, L. Lonergan, T. Weight and N. White for their help. N. Schofield, T. Sømme, and two anonymous people are thanked for their insightful reviews.

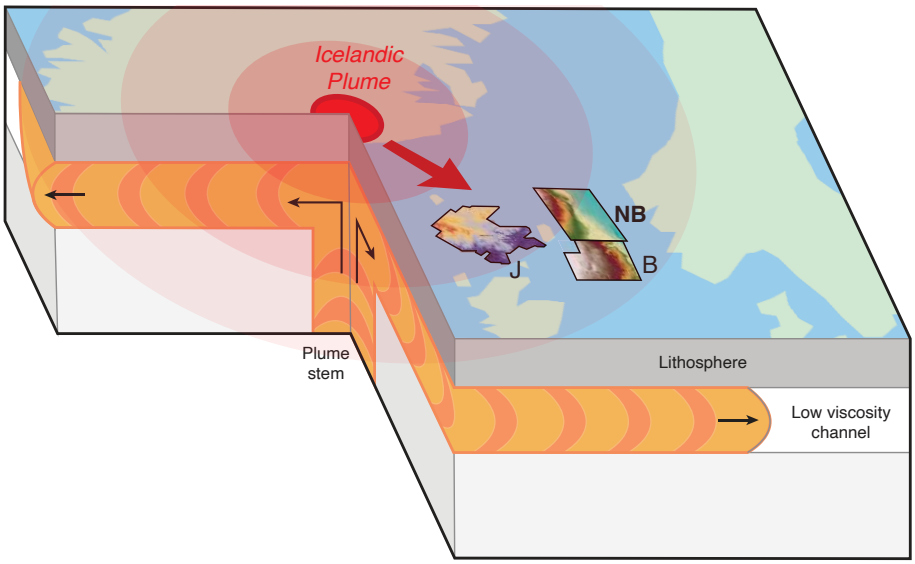


Figure 9: **Schematic of geodynamics in the Bressay region and its surroundings at $\sim 55-58$ Ma.** Red spot = Icelandic plume (IP) at $\sim$ 55 Ma (White & McKenzie, 1989). Oversized polygons indicate locations of now-buried terrestrial landscapes coloured by height: J = Judd (Shaw Champion et al., 2008; Hartley et al., 2011), B = Bressay (Underhill, 2001; Stucky de Quay et al., 2017), NB = North Bressay (this study). Study site outlines are considerably enlarged for clarity. Orange layer = idealized plume head spreading radially; large excess temperatures are indicated by pink Poiseuille flow velocity profiles. Black arrows = direction of plume flow. Red arrow = planform radial plume flow towards study region. Red shaded polygons = positions of buoyant thermal anomalies beneath the North Atlantic.

## References


Christensen, N. (1982). Seismic velocities, Handbook of Physical Properties of Rocks, II RS Carmichael, 1–228.

Conway-Jones, B. W., & White, N. (2022). Paleogene buried landscapes and climatic aberrations triggered by mantle plume activity. *Earth and Planetary Science Letters*, *593*, 117644. doi:10.1016/j.epsl.2022.117644.

Czarnota, K., Hoggard, M., White, N., & Winterbourne, J. (2013). Spatial and temporal patterns of Cenozoic dynamic topography around Australia. *Geochemistry, Geophysics, Geosystems*, *14*, 634–658.

Hardman, J. P. A., Schofield, N., Jolley, D. W., Holford, S. P., Hartley, A. J., Morse, S., Underhill, J. R., Watson, D. A., & Zimmer, E. H. (2018). Prolonged dynamic support from the icelandic plume of the ne atlantic margin. *Journal of the Geological Society*, *175*, 396–410. doi:10.1144/jgs2017-088.

Hartley, R. A., Roberts, G. G., White, N., & Richardson, C. (2011). Transient convective uplift of an ancient buried landscape. *Nature Geoscience*, *4*, 562.

Hoggard, M. J., White, N., & Al-Attar, D. (2016). Global dynamic topography observations reveal limited influence of large-scale mantle flow. *Nature Geoscience*, *9*, 456.

Howard, A. D., Dietrich, W. E., & Seidl, M. A. (1994). Modeling fluvial erosion on regional to continental scales. *Journal of Geophysical Research: Solid Earth*, *99*, 13971–13986.

Japsen, P., & Chalmers, J. A. (2000). Neogene uplift and tectonics around the North Atlantic: overview. *Global and Planetary Change*, *24*, 165–173.

Jolley, D. W., Millet, J. M., Schofield, N., Broadley, L., & Hole, M. J. (2021). Stratigraphy of volcanic rock successions of the North Atlantic rifted margin: the offshore record of the Faroe–Shetland and Rockall basins. *Earth and*

*Environmental Science Transactions of the Royal Society of Edinburgh*, *112*, 61–88.

Jones, S. M., & White, N. (2003). Shape and size of the starting Iceland plume swell. *Earth and Planetary Science Letters*, *216*, 271–282.

Jones, S. M., White, N., & Maclennan, J. (2002). V-shaped ridges around Iceland: Implications for spatial and temporal patterns of mantle convection. *Geochemistry, Geophysics, Geosystems*, *3*, 1–23.

Lawver, L. A., & Müller, R. D. (1994). Iceland hotspot track. *Geology*, *22*, 311–314.

Luterbacher, H., Ali, J., & Brinkhuis, H. (2004). The Paleogene Period: pp. 384–408 in FM Gradstein, JG Ogg, and AG Smith (eds.), A Geologic Time Scale 2004.

Mackay, L., Turner, J., Jones, S., & White, N. (2005). Cenozoic vertical motions in the Moray Firth Basin associated with initiation of the Iceland Plume. *Tectonics*, *24*.

Mudge, D., & Bujak, J. (2001). Biostratigraphic evidence for evolving palaeoenvironments in the Lower Paleogene of the Faeroe–Shetland Basin. *Marine and Petroleum Geology*, *18*, 577–590.

Mudge, D. C. (2015). Regional controls on Lower Tertiary sandstone distribution in the North Sea and NE Atlantic margin basins. *Geological Society, London, Special Publications*, *403*, 17–42.

Mudge, D. C., & Jones, S. M. (2004). Palaeocene uplift and subsidence events in the Scotland–Shetland and North Sea region and their relationship to the Iceland Plume. *Journal of the Geological Society*, *161*, 381–386.

Parker, R. L. (1994). *Geophysical Inverse Theory*. Princeton University Press.

Parnell-Turner, R., White, N., Henstock, T., Murton, B., Maclennan, J., & Jones, S. M. (2014). A continuous 55-million-year record of transient mantle plume activity beneath Iceland. *Nature Geoscience*, *7*, 914.

Pritchard, D., Roberts, G., White, N., & Richardson, C. (2009). Uplift histories from river profiles. *Geophysical Research Letters*, *36*.

Stucky de Quay, G., Roberts, G. G., Watson, J. S., & Jackson, C. A.-L. (2017). Incipient mantle plume evolution: Constraints from ancient landscapes buried beneath the North Sea. *Geochemisty, Geophysics, Geosystems*, *18*, 973–993.

Rickers, F., Fichtner, A., & Trampert, J. (2013). The Iceland–Jan Mayen plume system and its impact on mantle dynamics in the North Atlantic region: evidence from full-waveform inversion. *Earth and Planetary Science Letters*, *367*, 39–51.

Roberts, G. G., & White, N. (2010). Estimating uplift rate histories from river profiles using African examples. *Journal of Geophysical Research: Solid Earth*, *115*.

Rosenbloom, N. A., & Anderson, R. S. (1994). Hillslope and channel evolution in a marine terraced landscape, Santa Cruz, California. *Journal of Geophysical Research: Solid Earth*, *99*, 14013–14029.

Rudge, J. F., Shaw-Champion, M. E., White, N., McKenzie, D., & Lovell, B. (2008). A plume model of transient diachronous uplift at the Earth's surface. *Earth and Planetary Science Letters*, *267*, 146–160.

Saunders, A., Fitton, J., Kerr, A., Norry, M., & Kent, R. (1997). The north Atlantic igneous province. *Large igneous provinces: Continental, oceanic, and planetary flood volcanism*, (pp. 45–93).

Schoonman, C., White, N., & Pritchard, D. (2017). Radial viscous fingering of hot asthenosphere within the Icelandic plume beneath the North Atlantic Ocean. *Earth and Planetary Science Letters*, *468*, 51–61.

Sclater, J. G., & Christie, P. A. (1980). Continental stretching: An explanation of the post-Mid-Cretaceous subsidence of the central North Sea Basin. *Journal of Geophysical Research: Solid Earth*, *85*, 3711–3739.

Shaw Champion, M., White, N., Jones, S., & Lovell, J. (2008). Quantifying transient mantle convective uplift: An example from the Faroe-Shetland basin. *Tectonics*, *27*.

Smallwood, J. R., & Gill, C. E. (2002). The rise and fall of the Faroe–Shetland Basin: evidence from seismic mapping of the Balder Formation. *Journal of the Geological Society*, *159*, 627–630. doi:10.1144/0016-764902-064.

Storey, M., Duncan, R. A., & Tegner, C. (2007). Timing and duration of volcanism in the North Atlantic Igneous Province: Implications for geodynamics and links to the Iceland hotspot. *Chemical Geology*, *241*, 264–281.

Tarboton, D. G. (1997). A new method for the determination of flow directions and upslope areas in grid digital elevation models. *Water resources research*, *33*, 309–319.

Underhill, J. (2001). Controls on the genesis and prospectivity of Paleogene palaeogeomorphic traps, East Shetland Platform, UK North Sea. *Marine and Petroleum Geology*, *18*, 259–281.

Whipple, K. X., & Tucker, G. E. (1999). Dynamics of the stream-power river incision model: Implications for height limits of mountain ranges, landscape response timescales, and research needs. *Journal of Geophysical Research: Solid Earth*, *104*, 17661–17674.

White, N. (1990). Does the uniform stretching model work in the North Sea. *Tectonic evolution of the North Sea rifts*, *181*, 217–239.

White, R., & McKenzie, D. (1989). Magmatism at rift zones: The generation of volcanic continental margins and flood basalts. *Journal of Geophysical Research: Solid Earth*, *94*, 7685–7729.

Wyllie, M. R. J., Gregory, A. R., & Gardner, L. W. (1956). Elastic wave velocities in heterogeneous and porous media. *Geophysics*, *21*, 41–70.